Journal of Power Sources 273 (2015) 1136–1141

Contents lists available at ScienceDirect

Journal of Power Sources

journal homepage: www.elsevier.com/locate/jpowsour

Li_2S cathode modified with polyvinylpyrrolidone and mechanical milling with carbon

Jun Liu [a], Hiroki Nara [b], Tokihiko Yokoshima [b], Toshiyuki Momma [a, b], Tetsuya Osaka [a, b, *]

[a] Graduate School of Advanced Science and Engineering, Waseda University, Japan
[b] Faculty of Science and Engineering, Waseda University, Okubo 3-4-1, Tokyo 169-8555, Japan

HIGHLIGHTS

- The Li_2S-C-PVP electrode with 60 wt% Li_2S was prepared.
- PVP helps to increase the capacity of Li_2S, but retards its charge transfer.
- Carbon mixture in Li_2S-C facilitates the initial activation of Li_2S.

ARTICLE INFO

Article history:
Received 16 July 2014
Received in revised form
19 September 2014
Accepted 30 September 2014
Available online 13 October 2014

Keywords:
Li_2S-C
Lithium sulfide
Polyvinylpyrrolidone (PVP)
Polyethylene oxide (PEO)
Mixed binder

ABSTRACT

Polyvinylpyrrolidone (PVP) is used with polyethylene oxide (PEO) as a mixed binder for mechanically milled Li_2S. PVP demonstrates its advantage in terms of increasing the capacity of Li_2S, but boosts the potential barrier at the beginning of the first charge. It is also revealed that PVP retards the charge-transfer kinetics of Li_2S. In Li_2S-C prepared by mechanical milling, carbon compensates for the electrochemical insulation of the PVP binder and improves the cycle stability. As a result, the Li_2S-C-PVP electrode with 60 wt% Li_2S content displays a low potential barrier at the onset of charge and a stable capacity of about 460 mAh g^{-1} at 0.1 C.

1. Introduction

With the ever-increasing markets for advanced portable electronics, electric vehicles, and stationary energy storage systems, there is a strong and urgent demand for rechargeable batteries with high specific energy. Current oxide-based cathodes of lithium ion batteries with relatively low practical capacities are still the limiting factor. Therefore, much attention is presently devoted to Li_2S, with a high theoretical capacity of 1166 mAh g^{-1}, which is almost four times the limit for commercial oxide-based cathodes [1,2]. Moreover, Li_2S is attractive for battery fabrication from the view point of the usage of a lithium-free anode, unlike with the sulfur cathode used in the common Li-S system. The practical application of Li_2S has been hindered to date by a series of shortcomings: low electronic conductivity, low lithium ion diffusivity, and dissolution of polysulfides into the electrolyte. Among these shortcomings, the dissolution of polysulfides, which results in a loss of active materials and the well-known shuttle effect, is the key challenge [3–5]. Current methodologies to address the aforementioned issues can be sorted into two categories. The first kind of method focuses on the carbonaceous-shell encapsulated Li_2S [6–11], in an attempt to limit polysulfide dissolution and improve the overall conductivity. The second methodology is innovation in terms of the electrolyte, with studies including polysulfide saturated electrolyte [12], electrolyte with highly concentrated lithium salt [13], polymer electrolyte [1], and solid-state electrolyte [14,15]. Even though great progress has been made in these researches, a low cost and highly efficient method for the preparation of Li_2S cathode has yet to be discovered. Recently, Y. Cui et al. reported a promising Li_2S cathode on carbon fiber paper simply by using innovative polyvinylpyrrolidone (PVP) binder [16]. Another simple method was also reported by S. Meini et al.; in their study, the use of the redox mediator decamethylferrocene enabled the Li_2S cathode (59 wt% Li_2S content) to achieve a capacity of 500 mAh g^{-1} after 150 cycles [17].

* Corresponding author. Graduate School of Advanced Science and Engineering, Waseda University, Japan.
E-mail address: osakatets@waseda.jp (T. Osaka).

http://dx.doi.org/10.1016/j.jpowsour.2014.09.179
0378-7753/

In this work, we aim to prepare a Li_2S electrode with high Li_2S content of 60 wt% through a simple method. PVP and polyethylene oxide (PEO) mixed binders are used for Li_2S electrode. The PVP polymer is selected as it has been reported to be effective in anchoring lithium polysulfide and preventing its dissolution into the electrolyte through its strong interaction with lithium atoms [16]. Furthermore, the PEO binder is expected to build a lithium ion diffusion path in the dense electrode. However, the strong affinity of PVP for lithium atoms of Li_2S makes it unfavorable for lithium ions diffusion. The insulating PVP may also act as barrier for electron transport when it covers the surface of Li_2S. Therefore, in order to improve the slowed kinetics that is expected to be caused by PVP, mechanical milling of Li_2S with carbon is performed (together with the use of PVP). The influences of PVP with and without mechanical milling with carbon on the electrochemical reactions of Li_2S were studied by cyclic voltammetry and electrochemical impedance spectroscopy.

2. Experimental

2.1. Preparation of Li_2S, Li_2S-PVP, and Li_2S-C-PVP electrodes

Mechanically milled Li_2S particles (MM Li_2S) were prepared from commercial Li_2S (98%, Wako) by high-energy mechanical milling (Retsch Mixer Mill MM400) for 8 h with a shaking frequency of 25 s^{-1}. Stainless steel balls of diameter 10 mm were used as the milling medium. The weight ratio between the milling balls and commercial Li_2S was set to 10:1. To prevent overheating of the system, we added a rest time of 20 min after each hour of ball milling. Li_2S-C particles were prepared in a similar way to that described in our previous report [18]. Here, commercial Li_2S and ketjen black (KB) with a weight ratio of 80:20 were subjected to high-energy mechanical milling for 8 h under the same conditions as for MM Li_2S.

For the formation of the Li_2S electrode, MM Li_2S, acetylene black (AB), and PEO (M_w = 600,000, Aldrich) were mixed with a weight ratio of 60:25:15. After being mixed in acetonitrile and stirred for 8 h, the well-dispersed viscous slurry was cast by using a doctoral blade (SNC-280, Yasui Seiki Co. LTD) onto aluminum foil in a dry-room with a dew point less than −50 °C. Subsequently, the electrode was heated at 60 °C for 5 h inside an Ar-filled glove box. The Li_2S electrode had a Li_2S mass loading of 0.8 mg cm^{-2}.

For the preparation of the Li_2S-PVP electrode, MM Li_2S particles, AB, PVP (M_w = 360,000, Wako) and PEO with a weight ratio of 60:25:10:5 were used. The slurry and the electrode were prepared in the same way as for the Li_2S electrode. The mass loading of Li_2S in the Li_2S-PVP electrode was ~1.5 mg cm^{-2}.

For the production of the Li_2S-C-PVP electrode, Li_2S-C, AB, PVP and PEO were mixed with a weight ratio of 75:10:10:5 so that the content of Li_2S in the electrode was 60 wt%. The slurry and the electrode were also prepared similarly to the Li_2S electrode. The mass loading of Li_2S in the Li_2S-C-PVP electrode was also ~1.5 mg cm^{-2}.

2.2. Electrochemical measurements

The three electrodes were punched into circular pieces of diameter 9 mm for cell assembly. Coin cells (2032 type) were prepared with lithium metal anode and polypropylene separator (Celgard 2500). For the electrolyte, lithium trifluoromethane sulfonate ($LiCF_3SO_3$, Aldrich, 99.995%) and tetraethyleneglycol dimethylether (TEGDME, Aldrich, 99%) were mixed in molar ratio of 1:4 with the addition of 1 wt% $LiNO_3$. Constant-current charging and discharging cycling tests were conducted using a charge–discharge system (TOSCAT-3100, Toyo system). The initial first cycle was tested at a 0.05 C, by charging to different high cutoff voltages for the three electrodes and followed by discharging to 1.5 V vs Li/Li^+. A 0.1 C rate was used thereafter in the voltage range of 3.0–1.5 V. For the Li_2S-PVP electrode, the first charge step time was capped at 15 h because a high cutoff voltage of 4.2 V was used. Cyclic voltammetry (CV) with a scan rate of 0.1 mV s^{-1} was conducted using electrochemical measurement equipment (HZ-5000, Hokuto Denko). Electrochemical impedance spectroscopy analysis was also performed with amplitude of 5 mV in the frequency range 200 kHz to 50 mHz by using an electrochemical instrument (VSP-300, BioLogic).

2.3. Morphological observation

Scanning electron microscopy (SEM) images were obtained by field–emission SEM (FE-SEM, S-4500S, Hitachi). The 50th cycled electrodes in the discharged state were washed with dimethoxyethane before SEM observation.

3. Results and discussion

Fig. 1 shows the CVs of the Li_2S electrode and Li_2S-PVP electrode. The CV measurements are initiated with a delithiation process by increasing the voltage from the open-circuit voltage. On the first anodic scan of the Li_2S electrode, the oxidation current begins from 3.70 V, as shown in Fig. 1a. As discussed extensively in the work of

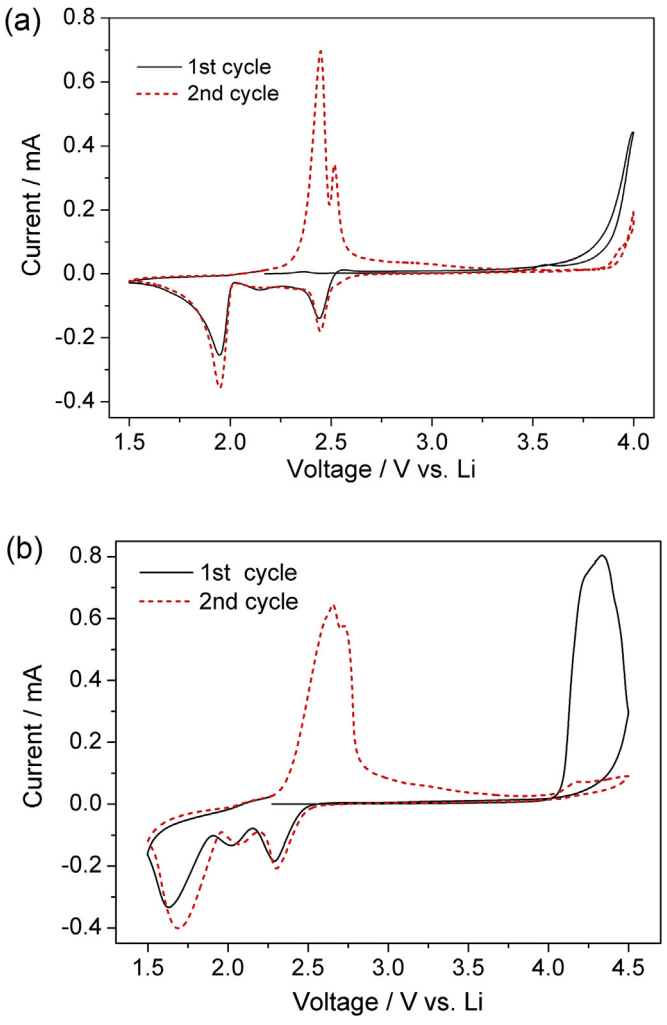

Fig. 1. Cyclic voltammograms (scan rate: 0.1 mV s^{-1}) for: (a) Li_2S electrode, (b) Li_2S-PVP electrode.

Yang et al. [12], Li_2S suffers from an initial potential barrier owing to the phase nucleation of polysulfides. The nucleation process for the new phase of polysulfides is difficult in Li_2S because of its poor electronic and ionic conductivity. Therefore, an over potential is needed to oxidize Li_2S. In the second cycle, the anodic peak of Li_2S electrode shifts negatively to a lower voltage of 2.45 V. This means that the high polarization, from which the Li_2S electrode suffers at the initial charge, subsequently decreases. According to the literature [12,19], once the oxidation of Li_2S initiates, the polarization process decreases instantly through the generation of soluble polysulfide ions. During the cathodic scans, three peaks are observed at about 2.45, 2.1 and 1.95 V. These peaks correspond to the stepwise reduction of S_8 to long-chain polysulfides (Li_2S_n, $n = 5–8$), long-chain to short-chain polysulfides (Li_2S_n, $n = 2–4$), and short-chain polysulfides to Li_2S, respectively [20]. These reduction peaks exhibit increased peak density in the second cycle because the Li_2S active materials are not oxidized completely in the first cycle owing to the limited scanning range. In contrast, Fig. 1b shows that the first anodic peak of the Li_2S-PVP electrode starts from a very high voltage of 4.00 V and centers at 4.25 V. The higher oxidation peak in the Li_2S-PVP electrode can be attributed to the strong affinity of PVP for Li_2S [16,21], which makes the lithium ion migration for the phase nucleation of polysulfides more difficult. In the second cycle, the anodic peak of the Li_2S-PVP electrode also shifts negatively to 2.60 V after the nucleation of polysulfides, compared with 2.45 V for the Li_2S electrode. The higher anodic peak of Li_2S-PVP electrode in the second cycle also reflects the influence of PVP on the over potential for the oxidization process. In the cathodic scans of the Li_2S-PVP electrode, three reductive peaks are located at 2.3 V, 2.07 V and 1.7 V, and are broader than those of the Li_2S electrode; this is indicative of a lower rate of Li^+ uptake in the Li_2S-PVP electrode with higher mass loading of active materials.

The initial charge and discharge profiles of the Li_2S-PVP and Li_2S electrodes are presented in Fig. 2a. The voltage increases abruptly at the onset of charging in both electrodes. The Li_2S-PVP electrode climbs quickly to 4.16 V, which is consistent with its initial anodic peak in the CV plots, and then maintains a high plateau; on the other hand, the Li_2S electrode exhibits an over potential hump with its peak at 3.65 V, which corresponds to the oxidization current in the first anodic CV scan. As mentioned above, the origin of the high polarization for Li_2S is thought to be the phase nucleation of polysulfides [12]. The higher over potential in the Li_2S-PVP electrode indicates that PVP makes the phase nucleation of polysulfides more difficult because of the strong affinity between the oxygen double bonding in PVP and the lithium ion. PVP addition may also account for the maintaining of the high charge plateau near 4 V in the Li_2S-PVP electrode after the abrupt voltage increase, in contrast to the charge plateau at 2.5 V for the Li_2S electrode following its voltage hump. Furthermore, the Li_2S-PVP electrode has a much higher charge–discharge capacity than the Li_2S electrode without PVP. This indicates that PVP helps to increase the capacity. Because PVP would help anchor the polysulfides from dissolution due to its strong affinity for Li_2S and lithium polysulfides, the remained polysulfides in the electrode can react with lithium ion further to achieve increased capacity. Fig. 2b shows the second charge–discharge profiles of the Li_2S-PVP and Li_2S electrodes. The voltage hump at the beginning of charge disappears in both electrodes. Interestingly, the Li_2S-PVP electrode still displays a higher voltage of charging plateau than the Li_2S electrode, in agreement with the CV results. As a result, the voltage hysteresis ΔV_2 of the Li_2S-PVP electrode is larger than ΔV_1 of the Li_2S electrode. This means that PVP is electrochemically unfavorable for Li_2S. Fig. 2c shows the Nyquist plot of Li_2S-PVP electrode, which is composed of one depressed semicircle in the high frequency region and one straight line in the low frequency region. With electrochemical activation of 4.16 V, the diameter of the semicircle, which corresponds to the charge transfer resistance at the interface, decreases. The improved charge-transfer kinetics result from the phase

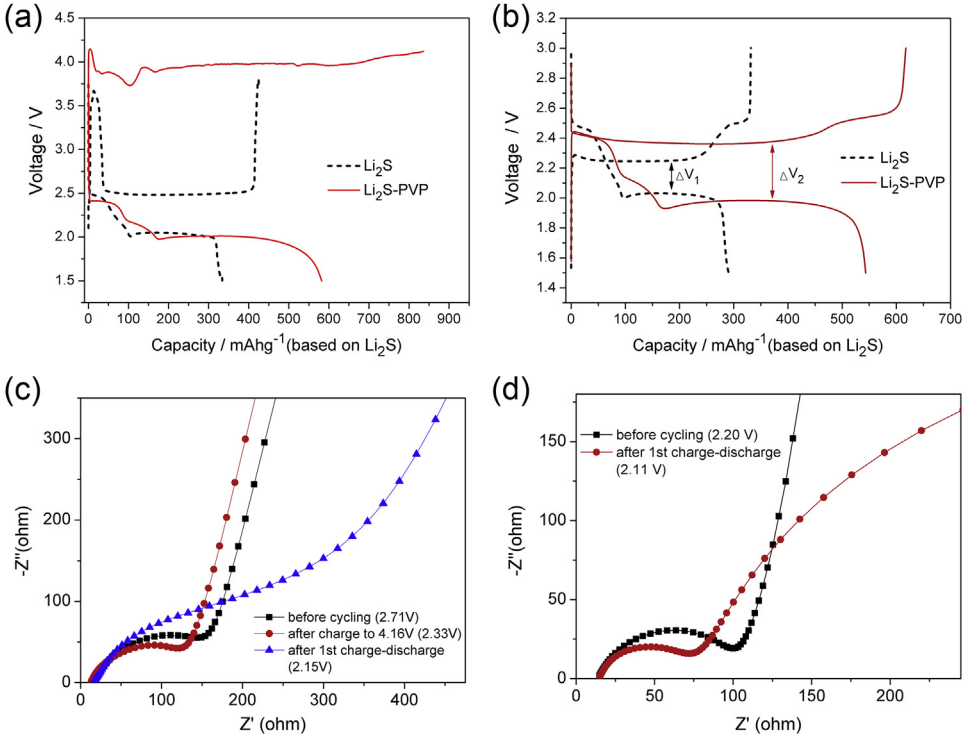

Fig. 2. Comparison of the charge–discharge curves of the Li_2S-PVP electrode (4.2 V cutoff) and Li_2S electrode (3.8 V cutoff): (a) 1st charge–discharge at 0.05 C (58.3 mAh g^{-1}), (b) 2nd charge–discharge at 0.1 C (116.6 mAh g^{-1}). Impedance spectra (with open-circuit voltage presented in parenthesis) for: (c) Li_2S-PVP electrode and (d) Li_2S electrode.

nucleation of polysulfide under the over potential of 4.16 V; it is reported in the literature that the formation of soluble polysulfide can reduce the charge transfer resistance through the enhanced active sites and facile accessibility of active species from the electrolyte [19]. After the first delithiation and lithiation, an extended arc is observed in the high and medium frequency range, implying significantly increased charge transfer resistance. A similar phenomenon is reported at the dense sulfur cathode after the completion of discharge owing to high tortuosity of dense electrode [19]. Another explanation for the increase in electrode impedance is that some discharge products (Li_2S_2/Li_2S) become inactive or isolated during the formation process owing to the loss of intimate contact with carbon [22]. In our case, the increased charge transfer resistance could be attributed to passivation of the electrode surface owing to the formation and/or rearrangement of solid discharged products on PVP. As shown in Fig. 2d, the Li_2S electrode represents a diameter of about 70 Ω for the semi-circle before cycling, which is smaller than that of the Li_2S-PVP electrode. Therefore, it is reasonable to conclude that PVP acts as barrier for electron and/or lithium transfer. Unlike the increased charge transfer resistance in the Li_2S-PVP electrode, the Li_2S electrode exhibits a decreased diameter of semi-circle after the first delithiation and lithiation, which is consistent with the reported results [7] and can be attributed to the porous structure formed after polysulfide dissolution and the available active species from the electrolyte. The opposite behavior of the Li_2S-PVP and Li_2S electrodes in terms of the change of semicircle from before cycling to after the first charge–discharge indicates that PVP is unfavorable for the electrode impedance. In the Li_2S electrode, the long linear tail at low frequency changes after the first delithiation and lithiation. This variation indicates that the microstructure of the Li_2S electrode changes because of the significant dissolution of polysulfide from the electrode.

As discussed above, PVP can improve the capacity of Li_2S, but at the same time, retards its charge transfer process. To retain the strength of PVP in Li_2S cathode, its use should be combined with another method that facilitates charge transfer. Thus, carbon modification of Li_2S through mechanical milling is applied together with the use of PVP aiming to improve the electron transfer of Li_2S as well as the capacity retention. Fig. 3a shows the CV of Li_2S-C-PVP electrode. A broad and large oxidation peak is observed on the first anodic scan, beginning from 2.70 V and centering at about 3.00 V; this corresponds to the oxidization of Li_2S to form sulfur. The voltage of this anodic peak is distinctly lower than that of the Li_2S-PVP electrode, which is seen at approximately 4.25 V. This indicates a much lower polarization because of the formation of intimate contact with carbon, which is enabled by ball milling. The improved electronic conductivity with carbon can facilitate the nucleation of polysulfides, and therefore, alleviate the polarization significantly compared with that of the Li_2S-PVP electrode. The second anodic peak at about 3.80 V could be assigned to undesired parasitic reactions. In the second cycle, the first large anodic peak of the Li_2S-C-PVP electrode also shifts negatively to 2.5 V for the same reason as described above. During the cathodic scans, similarly, three peaks are distinguishable at approximately 2.35, 2.10 and 1.85 V. As mentioned above, the lowest cathodic peak corresponds to the reductive formation of Li_2S and is mainly responsible for the discharge capacity. The Li_2S-C-PVP electrode displays this cathodic peak at 1.85 V, in contrast to the value 1.70 V for the Li_2S-PVP electrode. This means that the kinetics for the reductive formation of solid Li_2S during the lithiation process is improved in the Li_2S-C-PVP electrode because of the increased electronic conductivity.

Because the cyclic voltammogram of the Li_2S-C-PVP electrode shows two oxidation peaks on the first anodic scan, two different cutoff voltages at 3.60 and 3.80 V are applied, as seen in Fig 3b. The value of 3.60 V corresponds to the end of the first anodic peak, while the cutoff at 3.80 V accords with the second peak in the CV. At the onset of charging, over potential humps are also observed, but at a much lower voltage (2.70 V) than those of the Li_2S and Li_2S-PVP electrodes. This indicates that the increase in electronic

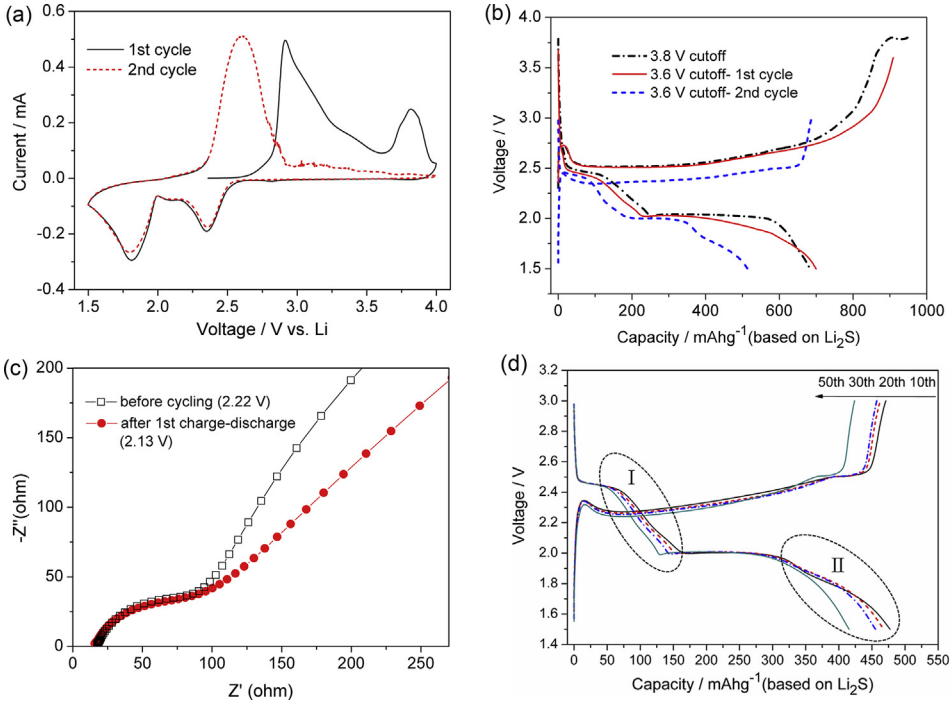

Fig. 3. (a) Cyclic voltammograms of Li_2S-C-PVP electrode. (b) Charge–discharge curves of Li_2S-C-PVP electrode with 3.80 and 3.60 V cutoffs at 0.05 C = 58.3 mAh g^{-1} (For 3.60 V cutoff, the 2nd cycle was tested at 0.1 C = 116.6 mAh g^{-1}). (c) Impedance spectra of Li_2S-C-PVP electrode with 3.60 V cutoff (Open-circuit voltage is presented in parenthesis). (d) Charge–discharge profile of Li_2S-C-PVP electrode over 50 cycles with 3.60 V cutoff in the first cycle.

conductivity caused by mechanical milling facilitates the initial phase nucleation of polysulfides. After the voltage hump, a long and slightly increased charge plateau, which is consistent with the large and wide first anodic peak in the CV, is observed with both the 3.60 and 3.80 V cut-offs. However, the latter shows a new oxidation plateau near 3.80 V, which corresponds to the second anodic peak during the first CV scan. This new plateau is attributed to undesired parasitic reactions related to the shuttling effect, which occurs only after the complete oxidization of Li_2S to sulfur [23]. At the first discharge, the 3.80 V cutoff displays a flat plateau at around 2.00 V compared to the arc curve of the 3.6 V cutoff. A possible explanation is that the redox shuttling reactions at 3.80 V cutoff brings about morphology changes on the surface of electrode. At the second charge of 3.60 V cutoff, the voltage hump almost disappears at the beginning of charge, and the following charge plateau appears at a lower voltage. Therefore, the charge curve seems to overlap with the discharge profile in the second cycle. To gain a further understanding of the electrochemical activation behavior brought about by mechanical milling with carbon, we employed EIS to characterize the cells, as shown in Fig. 3c. The Nyquist plot of the Li_2S-C-PVP electrode is also composed of one depressed semicircle in the high frequency region and one straight or curved line in the low frequency region. The diameter of the semicircle before cycling is almost the same as that of the Li_2S electrode (70 Ω), and smaller than that of the Li_2S-PVP electrode. Therefore, the increased charge transfer resistance caused by PVP addition in the Li_2S-PVP electrode is compensated by the mechanical milling with carbon in the Li_2S-C-PVP electrode. After the first charge and discharge, it displays a similar semicircle to that before cycling. This could be attributed to the stable structure achieved by the combined effect of mechanical milling with carbon and the addition of PVP.

Fig. 3d displays the charge–discharge profile of the Li_2S-C-PVP electrode at 0.1 C after 50 cycles. The charge–discharge profiles exhibit two charge plateaus and two discharge plateaus. It is interesting to note that the first charge plateau, which follows the small over potential hump, tends to decrease gradually with cycles. The decrease of charge plateau can be attributed to the gradually enhanced active sites inside the Li_2S-C-PVP electrode, which is caused by the slow dissolution of polysulfides during cycles. The discharge capacity fading mainly occurs in the slope range from 2.40 to 2.00 V (between the two discharge plateaus, marked by dashed circle I) and the arc curve from 1.90 to 1.50 V (after the second discharge plateau, marked by dashed circle II). Range I is related to the reduction of long-chain polysulfide to short-chain polysulfide, and Range II corresponds to the conversion of Li_2S_2 to Li_2S [24,25]. The capacity fading in Range I is due to the dissolution of polysulfide, which exhibits a gradual decrease with cycling. Furthermore, it appears that the Range II accounts for more significant capacity decay than Range I. It is clearly observed that the 50th cycle displays sharp drops at the end of discharge, in contrast to the 10th, 20th, and 30th cycles. This indicates that the solid conversion from Li_2S_2 to Li_2S is mainly responsible for the capacity fading upon long cycling.

The cycle performances of the Li_2S-C-PVP, Li_2S-PVP, and Li_2S electrodes measured under the current rate of 0.1 C are shown in Fig. 4. The Li_2S-C-PVP electrode exhibits less pronounced capacity fading than the Li_2S-PVP electrode. The improved cycle stability of the Li_2S-C-PVP electrode can be ascribed to the carbon mixture. KB acts as matrix and the polysulfides are adsorbed on the surface of the KB particles, thus alleviating the fast loss of active materials. The Li_2S-C-PVP electrode shows a capacity of about 460 mAh g^{-1} at 0.1 C with slow capacity fading. However, a large drop of capacity is observed in the initial cycle. The possible explanation comes from the big secondary particles of mechanically milled Li_2S-C (Fig. S(a)), which is larger than MM Li_2S (Fig. S(c)), shown as primary particles. During the dissolution of polysulfide in the initial cycle, which is accompanied by volume change, the aggregated Li_2S-C particles may break up and produce some isolated particles, therefore resulting in drastic capacity loss. Moreover, both the Li_2S-C-PVP and Li_2S-PVP electrodes outperform the Li_2S electrode in terms of capacity. This emphasizes the effect of PVP on increasing the capacity by immobilizing the polysulfide from dissolution into the electrolyte. All three samples show high coulombic efficiencies after the first two formation cycles.

Fig. 5 shows the morphology evolution of the Li_2S-C-PVP and Li_2S-PVP electrodes before charge and after the 50th cycle (after dissembling the cells in a glove box). Fig. 5a shows the disordered morphology of the Li_2S-C-PVP electrode before cycling. Many large Li_2S-C particles with a smooth surface and diameter from 2 to 10 μm are observed. A typical particle is marked by the black rectangle. There are also some aggregated granular particles, as outlined by the dashed yellow circle. These tiny particles are conductive carbon AB as confirmed by energy-dispersive X-ray spectroscopy (EDX). After the 50th cycle, these granular AB particles are no longer observed, but are replaced by large smooth particles, as seen in Fig. 5b. The EDX results (not shown) indicate that these particles covered on the surface are sulfur-rich materials. According to the literature [26,27], these deposited particles are probably insoluble Li_2S_2 or Li_2S, because insoluble discharge products are prone to be reduced from polysulfide at active sites in direct contact with the electrolyte. These cumulative sulfides would hinder the transportation of ions toward the inside of the cathode and result in induced passivation of the electrode surface, and finally, in capacity fading. This is partly supported by the quick voltage drop after the 2.00 V discharge plateau in the 50th charge–discharge profile of the Li_2S-C-PVP electrode (Fig. 3d), which reflects the passivation phenomenon [22]. From Fig. 5c, it is seen that before cycling, the Li_2S-PVP electrode displays a smooth morphology with some open pores. After 50 cycles, the precipitation of Li_2S_2/Li_2S is also observed, as marked by the dashed yellow circle in Fig. 5d. The other small area on the surface is also covered with thin solid film. In addition, the large crack observed in the electrode observed is probably caused by the repeated volume shrinkage and expansion during cycling. This volume change in the electrode may partly account for the fast capacity decay of the Li_2S-PVP electrode, as illustrated in Fig 4.

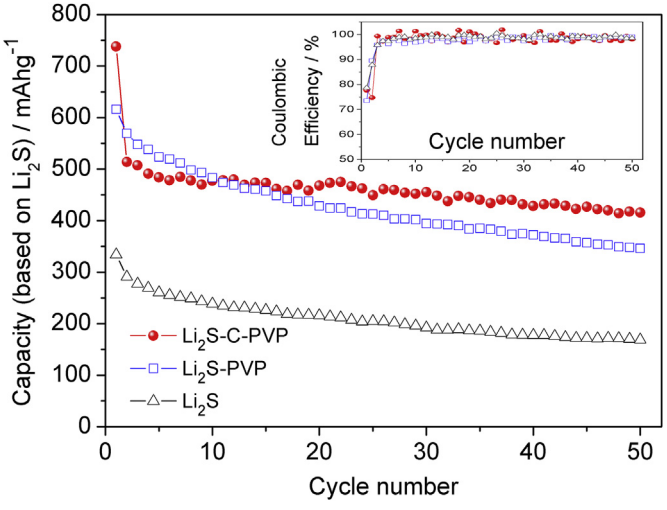

Fig. 4. 0.1 C capacity retention for Li_2S-C-PVP, Li_2S-PVP, and Li_2S electrodes (only the 1st cycle is 0.05 C = 58.3 mAh g^{-1}).

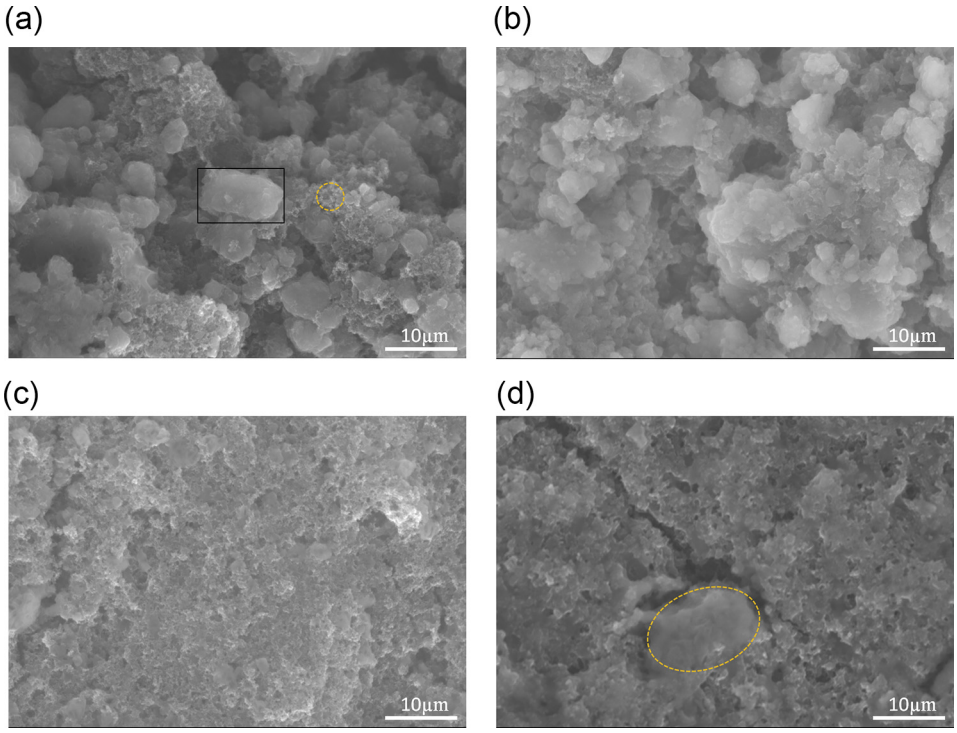

Fig. 5. SEM images: (a) Li_2S-C-PVP electrode before cycling; (b) Li_2S-C-PVP electrode after 50 cycles; (c) Li_2S-PVP electrode before cycling; (d) Li_2S-PVP electrode after 50 cycles.

4. Conclusion

In this study, we applied a PVP and PEO mixed polymer binder to Li_2S and Li_2S-C. The results showed that PVP is effective in improving the discharge capacity of Li_2S, but that this improvement comes at the expense of the charge transfer kinetics. Nevertheless, Li_2S-C, prepared by mechanical milling, compensates for the slowed charge transfer brought about by the use of PVP, and further improves the cycle stability. The Li_2S-C-PVP electrode with 60 wt% Li_2S displays a capacity of about 460 mAh g^{-1} at 0.1 C with slow capacity fading. This capacity is expected to be improved further by reducing the particle size of Li_2S-C. Moreover, SEM reveals that the formation of insoluble discharge products results in the occlusion of the active sites on the electrode surface, which may be responsible for the capacity decay upon long cycling. This problem remains a serious challenge for the achievement of a long cycle life, and is expected to be alleviated by enlarged cathode specific surface area. Further research on the modification of electrode surface is underway to improve the cycle performance of Li_2S cathode for further applications.

Acknowledgment

This work was supported partially by Advanced Low Carbon Technology Research and Development Program (JST-ALCA), Specially Promoted Research for Innovative Next Generation Batteries, and by the Grants for Excellent Graduate Schools (Practical Chemical Wisdom), MEXT, Japan.

Appendix A. Supplementary data

Supplementary data related to this article can be found at http://dx.doi.org/10.1016/j.jpowsour.2014.09.179.

References

[1] J. Hassoun, B. Scrosati, Angew. Chem. Int. Ed. 49 (2010) 2371–2374.
[2] Y. Yang, M.T. McDowell, A. Jackson, J.J. Cha, S.S. Hong, Y. Cui, Nano Lett. 10 (2010) 1486–1491.
[3] X. Ji, L.F. Nazar, J. Mater. Chem. 20 (2010) 9821–9826.
[4] B. Scrosati, J. Hassoun, Y.-K. Sun, Energy Environ. Sci. 4 (2011) 3287–3295.
[5] Y. Yang, G. Zheng, Y. Cui, Chem. Soc. Rev. 42 (2013) 3018–3032.
[6] J. Kim, J. Hassoun, S. Panero, Y.-K. Sun, B. Scrosati, Green 1 (2011) 323–328.
[7] K. Cai, M.-K. Song, E.J. Cairns, Y. Zhang, Nano Lett. 12 (2012) 6474–6479.
[8] J. Guo, Z. Yang, Y. Yu, H.D. Abruña, L.A. Archer, J. Am. Chem. Soc. 135 (2012) 763–767.
[9] S. Jeong, D. Bresser, D. Buchholz, M. Winter, S. Passerini, J. Power Sources 235 (2013) 220–225.
[10] K. Han, J. Shen, C.M. Hayner, H. Ye, M.C. Kung, H.H. Kung, J. Power Sources 251 (2014) 331–337.
[11] T. Takeuchi, H. Sakaebe, H. Kageyama, H. Senoh, T. Sakai, K. Tatsumi, J. Power Sources 195 (2010) 2928–2934.
[12] Y. Yang, G. Zheng, S. Misra, J. Nelson, M.F. Toney, Y. Cui, J. Am. Chem. Soc. 134 (2012) 15387–15394.
[13] F. Wu, A. Magasinski, G. Yushin, J. Mater. Chem. A 2 (2014) 6064–6070.
[14] M. Nagao, A. Hayashi, M. Tatsumisago, J. Mater. Chem. 22 (2012) 10015–10020.
[15] T. Takeuchi, H. Kageyama, K. Nakanishi, M. Tabuchi, H. Sakaebe, T. Ohta, H. Senoh, T. Sakai, K. Tatsumi, J. Electrochem. Soc. 157 (2010) A1196–A1201.
[16] Z.W. Seh, Q. Zhang, W. Li, G. Zheng, H. Yao, Y. Cui, Chem. Sci. 4 (2013) 3673–3677.
[17] S. Meini, R. Elazari, A. Rosenman, A. Garsuch, D. Aurbach, J. Phys. Chem. Lett. 5 (2014) 915–918.
[18] M. Agostini, J. Hassoun, J. Liu, M. Jeong, H. Nara, T. Momma, T. Osaka, Y.-K. Sun, B. Scrosati, ACS Appl. Mater. Interfaces 6 (2014) 10924–10928.
[19] C.S. Kim, A. Guerfi, P. Hovington, J. Trottier, C. Gagnon, F. Barray, A. Vijh, M. Armand, K. Zaghib, J. Power Sources 241 (2013) 554–559.
[20] Z. Yang, J. Guo, S.K. Das, Y. Yu, Z. Zhou, H.D. Abruna, L.A. Archer, J. Mater. Chem. A 1 (2013) 1433–1440.
[21] G. Zheng, Q. Zhang, J.J. Cha, Y. Yang, W. Li, Z.W. Seh, Y. Cui, Nano Lett. 13 (2013) 1265–1270.
[22] J. Zheng, M. Gu, C. Wang, P. Zuo, P.K. Koech, J.-G. Zhang, J. Liu, J. Xiao, J. Electrochem. Soc. 160 (2013) A1992–A1996.
[23] N. Azimi, W. Weng, C. Takoudis, Z. Zhang, Electrochem. Commun. 37 (2013) 96–99.
[24] Y.-X. Yin, S. Xin, Y.-G. Guo, L.-J. Wan, Angew. Chem. Int. Ed. 52 (2013) 13186–13200.
[25] S. Chen, F. Dai, M.L. Gordin, D. Wang, RSC Adv. 3 (2013) 3540–3543.
[26] M. He, L.-X. Yuan, W.-X. Zhang, X.-L. Hu, Y.-H. Huang, J. Phys. Chem. C 115 (2011) 15703–15709.
[27] L. Yuan, X. Qiu, L. Chen, W. Zhu, J. Power Sources 189 (2009) 127–132.